EXPERIENCES ABOUT THE COSMO-SKYMED STRIPMAP IMAGE DATA PROCESSING – FIRST RESULTS OF COSMO-SKYMED AO RESEARCH PROJECT

A. Losurdo[(1)], V. Sarli[(2)], A. Guariglia [(1)]

[(1)]GEOCART S.r.l., Viale del Basento 120, 85100 Potenza, Italy, Email:{a.losurdo / a.guariglia}@geocart.net
[(2)] Centro di Geomorfologia Integrata per l'area del Mediterraneo (CGIAM), Viale del Basento 120, 85100 Potenza, Italy, Email: v.sarli@cgiam.org

ABSTRACT

The use of COSMO-SkyMed data in the SAR interferometric techniques opens up new possibilities both for the monitoring of the surface deformation phenomena and the 3D measurements of the territory thanks to their height resolution.
GEOCART engineering company has developed an own software called "SLIDE" [1,2,3] (Sar Land Interferometry Data Exploitation) to process ERS SAR data in order to produce displacement maps of the territory by using the PSInSAR technique [4,5].
This paper presents the first results from the COSMO-SkyMed AO research project (ID-1380): "A software tool in order to process SAR stripmap data and calculate the deformation map with subcentimeter precision" regarding the adjustments of "SLIDE" to process COSMO data, and the first experiences on passive artificial Corner Reflectors (CRs).

1. TEST SITE AND DATA SET

Two test sites in the Basilicata region (Southern Italy) have been chosen for the project.

Figure 1. Descending "Agri-Pollino" scene (AP_DSC), ascending "Potenza" scene (PZ_ASC) in Google Earth Image. Basilicata Region (white colour) and Italy (green colour) indicated in the top - right square.

The former named "Agri-Pollino" is located in the south-west of the region and is historically subject to landslides. It includes the urban centres of Maratea, Lagonegro and Lauria.

Maratea is a village on the sea, it is called "the pearl of the Tyrrhenian Sea" for the beautiful panorama. Maratea's urban centre is placed in a smoothly sloping valley behind two mountains at north-west and south-east.
The second test site called "Potenza" because municipality of Potenza is localized in the centre of the frame. The "Potenza" frame covers the area where prototypal passive Corner Reflectors (CRs) were tested and where, subsequently, ten pairs of CRs have been installed. The interferometric multitemporal datasets of COSMO-SkyMed Stripmap Himage of level 1A are necessary to test "SLIDE" processing chain. These are characterized by a swath extension of about 40 km^2, a spatial resolution of 3x3 m^2 single look and polarization VV.
Moreover, the multitemporal data used are 13 in descending orbit with right look side and 33° incidence angle for the "AgriPollino" area, and 10 in ascending orbit with right look side and 48° incidence angle for "Potenza" area (Tab. 1.).

Table 1. COSM-SkyMed dataset used

"POTENZA" SCENE		"AGRI-POLLINO" SCENE	
DATE	SATELLITE	DATE	SATELLITE
20100914	CSKS1	20100518	CSKS2
20101125	CSKS2	20100713	CSKS1
20101126	CSKS3	20100721	CSKS2
20101203	CSKS1	20100806	CSKS2
20101211	CSKS2	20100830	CSKS1
20101219	CSKS1	20100907	CSKS2
20101227	CSKS2	20100915	CSKS1
20101228	CSKS3	20100923	CSKS2
20110104	CSKS1	20101009	CSKS2
20110112	CSKS2	20101017	CSKS1
		20101025	CSKS2
		20101118	CSKS1
		20101126	CSKS2

2. ANALISYS OF COSMO – SKYMED DATA

Interpolated and co-registered cut-outs, synthetic and differential interferograms, mean images and GTCs - Geocoded Terrain Corrected Data images - have been

produced in order to broaden the knowledge of COSMO-SkyMed data.
The high pixel resolution of SAR COSMO-SkyMed data with respect to ERS data arouses interest and is worth investigating.
The mean image (Fig. 2) made using 12 multitemporal cut-out data centred in Maratea appears very similar to an aerophotogrametric survey with a resolution of about 3-5 m.

Figure 2. Maratea Google's image and mean image produced with 12 "AgriPollino" frames (cut-out area has a surface of 2.5 x 3.0 km^2 (Lon x Lat))

The X-band of the COSMO-SkyMed system is more subject to atmospheric noise than ERS system. The shorter X-band wavelength brings about an increase in the fringes with respect to the ERS case. In addition, the highest pixel resolution causes a larger fragmentation of the coherent areas, and so a further noise.
The analysis has been made generating interferograms without any band filter on the image pairs.
It is interesting to compare the interferograms generated from the cut-outs of Maratea with the site of Pignola, a village near Potenza. For Maratea case the pairs of data used were characterized by a temporal baseline of eight days and very different normal baselines; while for Potenza, tandem (acquired with one day temporal baseline) and no-tandem pairs of data with very different normal baselines were used.
The interferometric phases (Fig. 3-4) exhibit the shape expected from the site orography and the orbital phase factor. In particular, it is possible to observe more speckle noise for the interferograms on Maratea than on Potenza. The fringes on Potenza's interferograms appear clear on the entire cut-outs without applying a low pass filter for the visualization that, instead, is necessary for Maratea case. The fringes are also visible in unfavourable cases as for example, that in the Fig. 4a (temporal baseline of 16 days and normal baseline of -446 meters).
All this confirms that the complexity of orography (Maratea case) affects the noise as ERS case. However, this noise can be partially eliminated by the DEM use in co-registration process [6,7]. Finally, the phase noise could be decreased if applying in a pre-processed step an adapted filter in azimuth direction and a common band filter in range particularly useful for the pairs characterized by a large normal baseline [8].

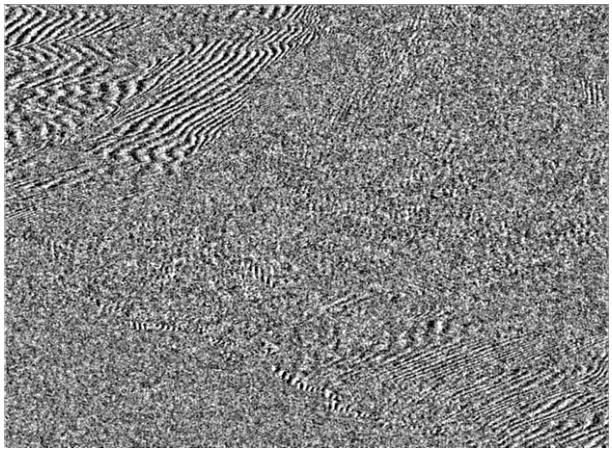

a) pair of 07-15/09/2010 with Bn about 491 m

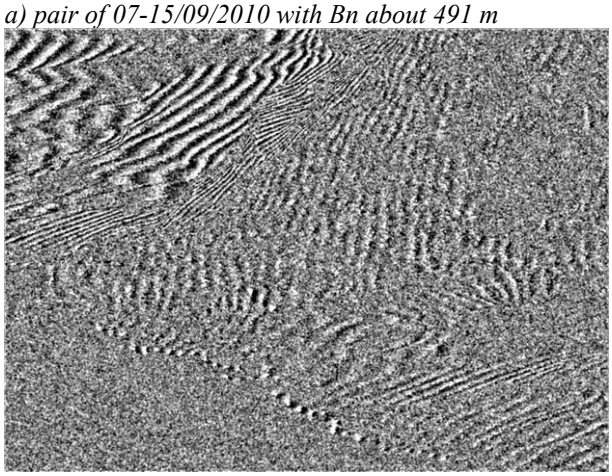

b) pair of 30/08 – 07/09/2010 with Bn about 232

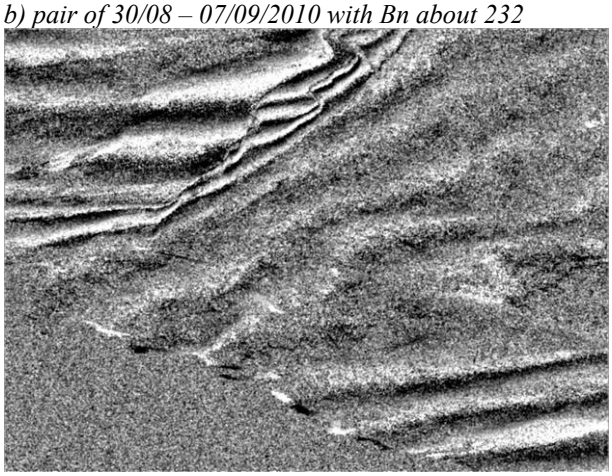

c) pair of 15 – 23/09/2010 with Bn about 28 m

Figure 3. Interferograms cut out in the Maratea area by using data pairs (a,b,c) with a temporal baseline of 8 days and different normal baselines. The visualizations were smoothed.

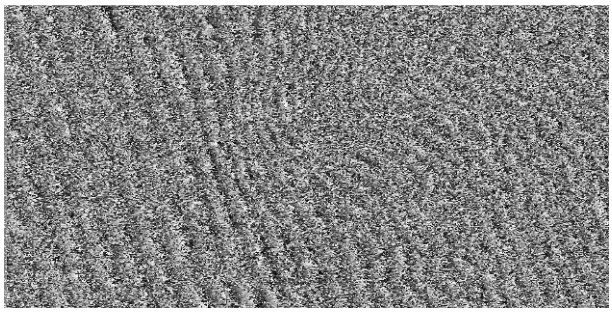

a) pair of 28/12/2010–13/01/2011 with Bn about -446m.

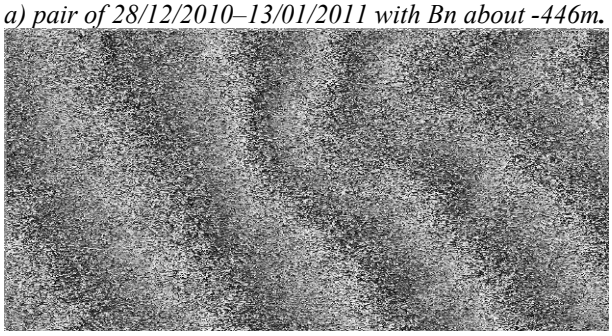

b) pair of 28-27/12/2010 with Bn about 70 m

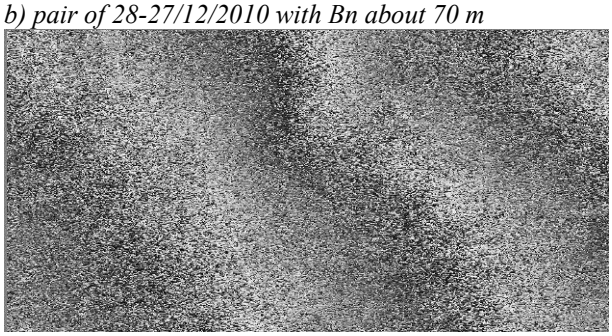

c) pair of 12-13/01/2011 with Bn about -38m

Figure 4. Interferograms cut out in Potenza area, generated by no tandem (a) and tandem image pairs (b and c). The visualizations were not smoothed.

GTCs (Geocoded Terrain Corrected, that is amplitude data projected on a regular grid in a cartographic system chosen) have been produced using own software code properly revised (see the following 3.1 and 3.2 paragraphs). These GTCs cover the Maratea and Potenza areas, the former using the DEM SRTM characterized by a resolution cell of 3x3 arcsec^2 and the latter using a Lidar DSM (Digital Surface Model) with a resolution of 2x2 m^2 (Fig. 5). It is important to note that it is necessary to make the DEM cell size similar to the Stripmap cell size (3x3 m^2) by interpolation or sampling process. The GTCs turned into a *.Kmz format have been overlapped on Google Earth, and the overlap is thought to be good but for a shift (x,y-axis translation) which has been evaluated. The shift may depend on many factors (any possible additional parameters unconsidered, inaccuracy of DEM and/or orbital State Vectors), further analysis will be made regarding it.

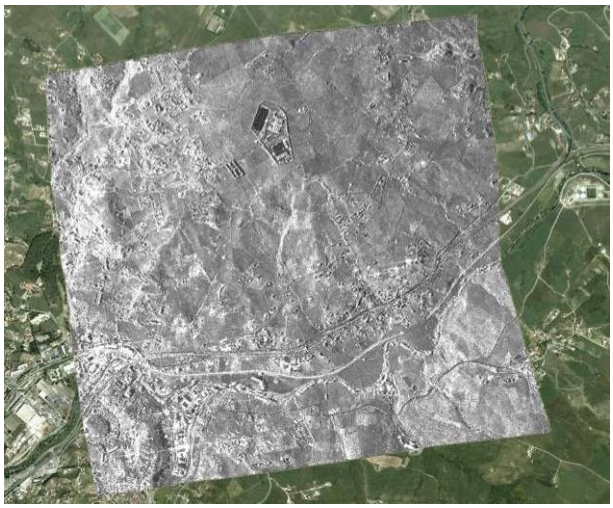

Figure 5. The GTC on Potenza area

3. ADJUSTMENT AND/OR TESTS OF "SLIDE" PROCEDURES

The SLIDE processing chain entails a first phase called "data stacking", which is characterized by steps regarding data cut-out and co-registration, the production of both differential interferograms and preliminary Point Target maps [5]. This part of SLIDE has been tested step by step and revised. Following, they present the most interesting algorithm adaptations and methods/products in order to estimate their validness.

3.1. Orbital module (adjustment)

The orbital module is aimed to calculate exactly pixel by pixel information on satellite-target distance, the corresponding geographic coordinates (by using a DEM) and perpendicular baselines. The orbital information to be used is represented by the State Vectors (SVs)/ECEF Satellite included in the metadata of the Stripmap Himage. These describe 15 orbital positions with geocentric coordinates, velocity, acceleration and acquisition time. By analyzing these, the orbit is assumed to be a part of a parabolic curve fitting the state vectors. Therefore, the orbit is simulated by three second order curves which describe the satellite motion in time in the three directions X,Y,Z.
Moreover, because the single Stripmap datum is acquired in about 16 seconds and the time interval between two subsequent state vectors is equal to 10 seconds, in order to optimize the orbital model module, a third-order SPLINE interpolation of the SVs has been introduced in the procedure. Thereby, the calculation function of the orbital curve is made by using the SVs calculated and falling into the acquisition interval increased by ± 2sec.

3.2. Automatic tiepoint and minimum satellite-ground point distance (test)

In more processes of the SLIDE interferometric chain it is necessary to geographically locate some ground points (called Ground Control Points) of the SAR image, or inversely, it is useful to associate the points of the SAR image processed to the geographical coordinates of the portion of the area represented. The automatic tiepoint is the algorithm that makes it.
In order to calculate the acquisition time of the ground point (GCP), the fundamental zero-Doppler concept is used, that is, it is acquired the time corresponding to the its minimum distance from the orbit trajectory (module of the minimum satellite-ground point distance [1]). In addition, the knowledge [1] of the row-column datum acquisition modalities allows us to localize the point.
An in-depth analysis of the ERS – COSMO-SkyMed case brings out the fact that as for the ERS data a calibration constant, K, equal to 24 metres [9] is used. It takes into account the signal delay in range caused by ERS electronic noise. As for the COSMO-SkyMed data, instead, no noise of the same nature is evidenced, so K equal to zero is used.

Good results have been obtained for the two modules (orbital module and automatic tiepoint). The SPLINE function introduced for the interpolation of the orbital metadata has significantly improved the cut-out precision in the azimuth direction. The test performed consists in doing pairs of cut-outs by using the simple orbital model used for ERS data (Fig. 6) and the orbital model optimized by SPLINE (Fig. 7). In this case Stripmap data relating to 18 May 2010 and 21 July 2010 were used.
In order to estimate the precision of the cut-out module, another test consisted in analyzing the overlap of the 13 multitemporal cut-outs in the same area of Maratea.
The procedure consisted in singling out a visible characteristic on the data, then localizing the pixel coordinates on a reference datum, and finally localizing the same characteristic on all the same dataset products. The shift found is included in the ± 3 pixel interval both in range and azimuth directions.

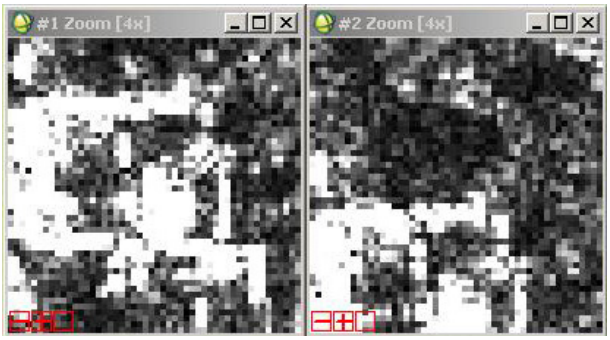

Figure 6. Cut-outs produced using simple orbital model

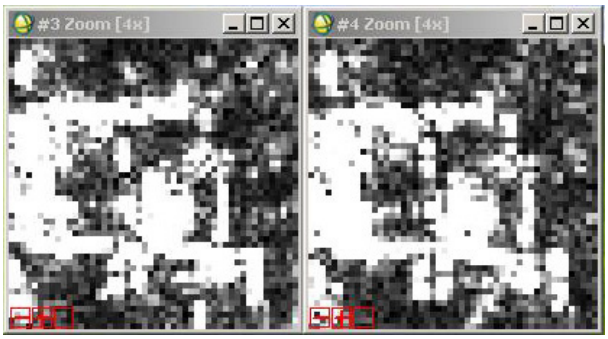

Figure 7. Cut-outs produced using SPLINE orbital model

3.3. Module for the production of Differential Interferograms (test)

The module for the production of differential interferograms utilizes the orbital module, the tiepoint module and the minimum satellite-ground point distance module. In this case the old procedure for ERS data has not been changed.
As for the multi-temporal differential interferograms produced on the sites of Maratea, Lauria and Potenza (Fig. 8-9), they show the features expected, that is, there are no interferometric fringes, therefore the subtraction orographic module applied is considered to be valid.

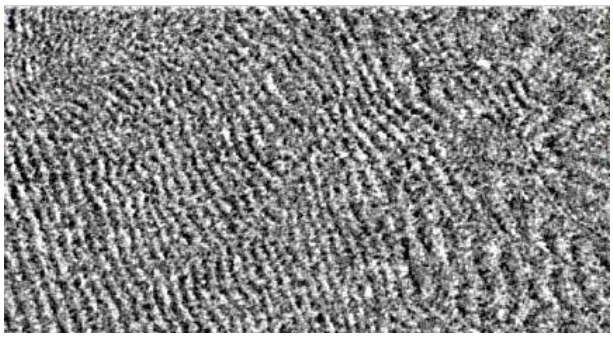
Figure 8. Interferogram of image pair of 28/12/2010 – 13/01/2011 with Bn = -446m. (Potenza area)


Figure 9. Differential interferogram of image pair of 28/12/2010 – 13/01/2011 with Bn = -446m. (Potenza area)

A further test performed on the differential interferometric data consisted in visualizing the

differential phase distribution with respect both to the perpendicular baselines and the time in correspondence with pairs of Point Targets (called PT) close to each other. In fact, in the ideal case of a perfect subtraction of the orographic and orbital components, the distributions expected depending on the perpendicular baselines are characterized by a linear regression line along zero axis, while in the real case, the dependence of the orographic component of differential phase with the elevation [10] allows us to estimate the altitude error of the DEM used, and the distribution expected is characterized by a linear or saw-toothed regression (in the case of major DEM orographic errors, Fig. 10). When the regression of the phase distribution vs. baselines develops along the zero x-axis, the expected phase distributions vs. time are characterized either by a linear regression along the zero x-axis (i.e. no displacement occurs, Fig. 11) or a linear or saw-toothed regression (i.e. displacement occurs). Therefore, by using the "SLIDE" visualization function, we report two examples of PT pairs performing as expected on the Maratea sites.

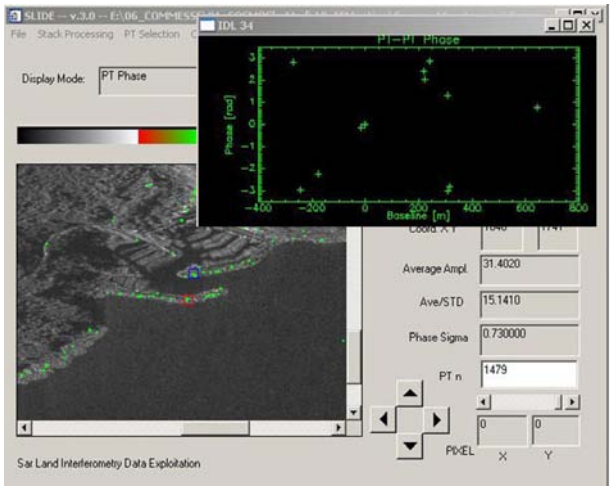

Figure 10. Phase distribution vs. perpendicular baseline of a PT pair on Maratea site: saw-toothed regression

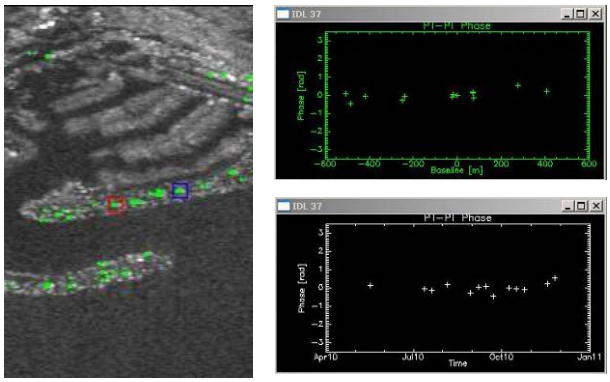

Figure 11. Phase distribution vs. perpendicular baseline and time of a PT pair on Maratea site: zero linear regression, that is no deformation

About the numerousness of PTs having a non-noisy distribution of the phases vs. the baselines distributed on zero x-axis or on a saw-toothed regression, it can be noted that when the graphs are characterized by a linear regression they are easy to read, on the contrary, when the graphs are characterized by a saw-toothed regression they are difficult to read. This could be due to:

1. the noise of the interferometric data;
2. the few points on the graph.

4. CORNER REFLECTORS

4.1. Design of prototypes

Passive CRs are coherent radar targets for their very high Radar-Cross-Section (RCS) compared their small sizes. The triangular trihedral is the most popular corner reflector thanks to the simplicity in the structural design and stability and manufacturing.

However, it has been shown that other shapes could be used for examples, rectangular (or square) or pentagonal, too [11]. The three most common types of corner reflector were taken into account: a dihedral with square plates and two trihedral, one with square plates and the other with triangular plates. The CRs to be used in this project must:

1. allow us to estimate ground motions (PS-InSAR);
2. be as cheap as possible.

Moreover, where possible, the CRs have to be installed in pairs in order to be visible along descending and ascending orbit. But at the same time, their overall dimensions should be as small as possible to guarantee a high mechanical stability (1st point), positioning accuracy and easiness of installation and un-installation.

To satisfy the 1st point the reflectors to be used must be detectable and easily visible in the different areas (rural, urban and industrial). The square trihedral and dihedral reflectors have been chosen because they have a max theoretical RCS higher than the triangular trihedral at same size. In addition, in order to recognize a CR in a SAR image, the difference between the backscattering coefficients of the corner reflector and its surroundings should be larger than 20 dB [12,9]. By analyzing the backscattering (on two data acquired before the CR installation) for the different area and in particular the responses of different buildings, the RCS can reach maximum values between about 10-15 dB (industrial area). Consequently, we have imposed a design RCS of about 40 dB considering the maximum RCS values of buildings and possible losses due to their orientation too.

On the basis of what described above and considering that in the aluminium market, a standard dimension of plates is 1500x3000 mm^2, we have chosen the plate size of 750x750 mm^2 for both the reflectors, so as to have no

material waste and to contain manufacturing costs through the uniform sizes (2nd point), too.
In order to have easiness of transport, installation and un-installation, both the prototypes are constituted by two frames with a structure manufactured by means of galvanized iron bars to improve stability (Fig. 12).

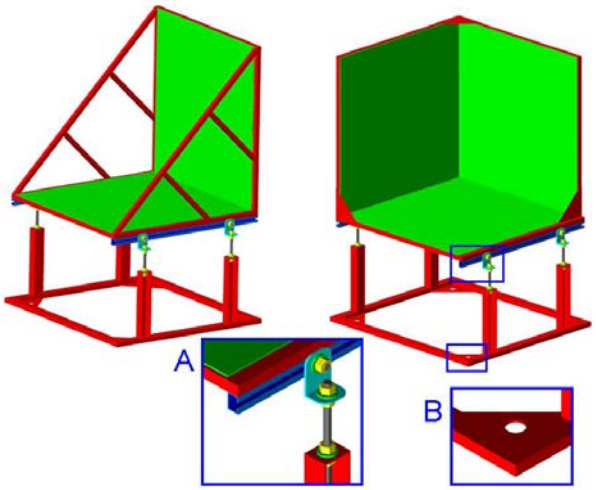

Figure 12. The two prototypes of CRs. A particular of the system in order to adjust elevation using a system consisting of guide rails, steel brackets, threaded rods, (A). A particular triangular steel plate perforated (B) to anchor the CRs.

The upper frame consists of the almond aluminium plates (the type of aluminium more readily available and used only for the prototypes, afterwards smooth aluminum plates were used for the production of 10 CRs) and it can be tilted to adjust the elevation thanks to a system consisting of guide rails, steel brackets, and threaded rods (Fig. 12, A). The steel brackets can slide along the guide rails making it possible raise the upper frame by threaded rods screwed to the steel brackets. The rods can run vertically inside the uprights of the base, in this way they can be lowered and raised to adjust the elevation. Moreover, the structure is reinforced and made more stable by cross galvanized steel braces for dihedral and triangular galvanized steel plates for trihedral (Fig.12). In addition, other bars are behind aluminium plates for both reflectors in order to prevent the plate bending especially in an environment where there is wind stress [13].
The lower frame is a robust base in order to support the upper frame and to anchor the whole system. Four triangular galvanized steel plates (Fig. 12, B) perforated have been welded in the inner corners of the base in order to fix it through headworks or screws.

4.2. Test of the prototype

The prototypes were tested in a rural area of the "Potenza" test site. The orientation data were carried out from the metadata of the Stripmap Himage. The azimuth is extracted from the attribute "scene orientation data" (counter-clockwise measured angle between the local north at scene centre and the opposite of the azimuth oriented direction) and the elevation was evaluated considering the near and far incidence angles.
The performance of CRs was evaluated by analyzing COSMO-SkyMed image. CRs can be readily identified without applying any stretch to the RCS image output display [14]. Their average RCS response on 8 images (Fig. 13) is about 25 dB for the dihedral (theoretical RCS ≅ 39 dB) and 30 dB for the trihedral CR (theoretical RCS ≅ 41 dB), against the average backscattering of background that is about -8/-9 dB on a 33x33 m^2 region of interest centered on positions of the CRs before their installations.

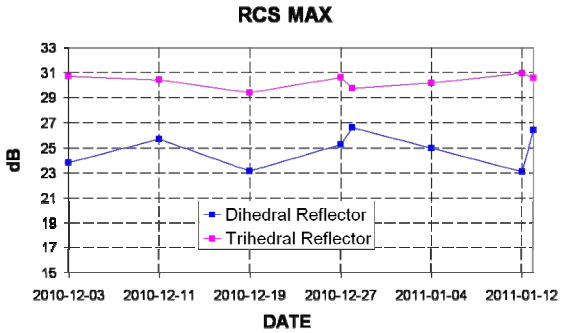

Figure 13. Experimental RCS values of the prototypal dihedral and trihedral corner reflector

It can be noted that the RCS values of the dihedral CR are smaller and more variable, and losses (vs the theoretical value) are major than the trihedral case. Consequently, the dihedral CR is more orientation-sensitive while trihedral CR has a more stable response as expected.
Nevertheless, the two prototypes are clear, strong, time persistent response targets as showed in the mean image (Fig. 14). In this figure, we can also note the response of a metal sheet roofing (indicated by MR).

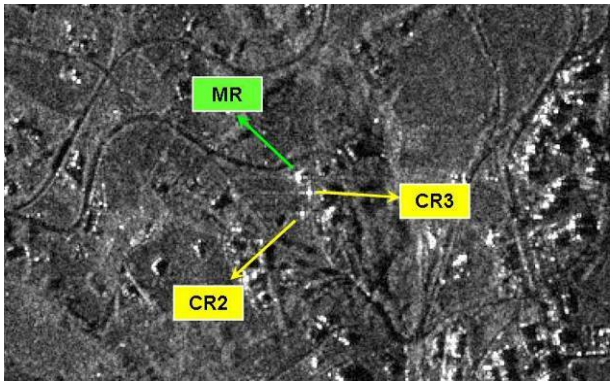

Figure 14. The mean image of test area, the prototypal reflectors are well visible: CR3 is the trihedral, CR2 is the dihedral and MR is the metal sheet roofing

4.3. Installation of CRs on different sites

Since the trihedral response is more stable and stronger, we decided to make eight pairs of trihedral reflectors and two pairs of dihedral reflectors to keep analyzing also the performance of the latter.
Thanks to their modular nature they were easily installed on both ground and prefabricated roof.

Figure 15. An example of the CR anchorage on the ground using headworks

Figure 16. An example of the CR anchorage on the concrete surface. A particular of resin adhesive used to stick the weight on the roof, on the top right.

In the first case (Fig. 15), in order to anchor them on the ground, we have used headworks with different heights depending on the type of soil without cement injection in order to reduce the environmental impact and to allow easy removal.
In the second case (Fig. 16), in order to anchor the CRs on the roof we have used concrete weight stuck on surface with a high performance elastic polyurethane resin adhesive (a particular is shown in the top left of Figure 16) so, without causing damage to the roof.

The azimuth orientation was set by mobile GPS geodetic station and the elevation was set by two levels placed orthogonally to each other.

5. CONCLUSIONS AND OUTLOOKS

This paper presents the first activities of the COSMO-SkyMed AO research project regarding the analysis of the COSMO-SkyMed products, the adjustments of an own tool software called SLIDE to process Stripmap Himage of COSMO-SkyMed data, and the first experiences on passive Corner Reflectors.
The main remarks are:

- The mean image produced by about 12 Stripmap Himage appears very similar to an aerophotogrametric survey. The synthetic and differential interferograms are characterized by a larger noise than the same products from the ERS data processing. This noise is partially due to the use of X band which is more subject to atmospheric noise, but principally, to a higher pixel resolution which makes the relating coherence map particularly discontinuous.
- The main adjustment about the SLIDE procedure has been made in the orbital model. In particular, a third-order spline interpolation of the State Vectors (ECEF Satellite position) has been introduced to increase State Vector positions falling into the acquisition interval of the scene. The validation of the procedures adjusted has been proved by accurate cut-outs and differential interferogram phases.
- The main features of the developed Corner Reflectors are their modular and flexible nature which allows a easy transport, an easy and accurate installation on different surface (e.g. ground or concrete roof), an orientation on different elevation and azimuth values, and an optimal stockpiling. All this has been obtained on the cheap in comparison with merchant price.

The next activities will be the adaptation of the other SLIDE procedures and the application of the “new” SLIDE on different sites. In particular, the application of SLIDE on sites where CRs are located will allow us to verify if they are suitable to be extracted on the Point Target map. At the same time, studies will be carried out in order to analyse RCS responses of the ten CRs and the factors that may affect them.

6. ACKNOWLEDGMENT

This work is funded by the Italian Space Agency (ASI) under "COSMO-SyMed Announcement of Opportunity" (ASI contract N. I/052/09/0).

7. REFERENCES

1. Marzo, C., Losurdo, A., Guerriero & Colangelo, A. (2005). Esperienze di utilizzo di tecnologie SAR nel calcolo del Digital Elevation Model e nel monitoraggio di strutture edilizie interessate da deformazioni del territorio. *Bollettino AIC*. No. 123-124-125, pp. 525-533.

2. Marzo, C., Losurdo, A., Leggeri, M., Colangelo, A., (2005). Applicazione delle tecniche interferometriche differenziali SAR per il monitoraggio degli spostamenti di fabbricati nella località di Maratea. *Atti Asita*. Vol II, pp. 453-459.

3. Losurdo, A., Pacifico, S., Sarli, V., Colangelo, A. & Leggeri, M. (2008). Integration of the differential SAR interferometry and ancillary GIS data for the study of the superficial deformations. *EARSeL eProceedings*. Vol. 7, No. 1, pp. 21-29.

4. Ferretti, A., Prati,C., & Rocca,F. (2001). Permanent Scatters in SAR Interferometry. *IEEE Trans. Geosci. Remote Sensing*. Vol. 39, No. 1, pp. 8-20.

5. Werner, C., Wegmuller, U., Strozzi, T. & Wiesmann, A. (2003). Interferometric Point Target Analysis for Deformation Mapping. *IGARSS'03*.

6. Arikan, M., Van Leijen, F., Guang, L., Hanssen, R. (2008). Improved image alignment under the influence of elevation. In Proc. *Fifth International Workshop on ERS/Envisat SAR Interferometry, 'FRINGE 2007'* (Eds. H. Lacoste & L. Ouwehand), ESA SP-649, ESA Publication Division, European Space Agency, Nordwijk.

7. Nitti, D. O., Hanssen,R.F., Refice, A., Bovenga, F., Milillo, G. & Nutricato, R. (2008). Evaluation of DEM-assisted SAR coregistration. *SPIE Europe Remote Sensing*. In Proc. of SPIE Vol. 7109 710919, pp. 1-14.

8. Fornaro, G., Monti Guarnieri, A. (2002). Minimum Square Error Space-Varying Filtering of Interferometric SAR Data. *IEEE Transactions on Geoscience and Remote Sensing*. Vol. 40, No. 1, pp. 11-21.

9. Curlander, J.C., 1991. Synthetic Aperture Radar: Systems and Signal Processing. Wiley-Interscience.

10. Adam, N., Kampes, B. & Eineder, M. (2003). The Development of a Scientific Permanent Scatterer System. *Proceedings of Joint Workshop ISPRS/EARSEL on High Resolution Mapping from Space*. Hannover 6-8 October, 2003.

11. Sarabandi, K. & Chiu, T., (1996). Optimum Corner Reflector For Calibration of Imaging Radars. *IEEE Transactions on antennas and Propagation*. Vol. 44, No. 10, pp. 1348 - 1361.

12. Xia, Y., Kaufmann, H. & Guo, X.F., (2004). Landslide Monitoring in the Three Gorges Area Using D-INSAR and Corner Reflectors. *Photogrammetric Engineering & Remote Sensing*. Vol. 70, No. 10, pp. 1167–1172.

13. Xia, Y., Kaufmann, H., Ge, X. F., & Yang, X. D. (2008). CR-Based TerraSAR-X Interferometry for Landslide Monitoring. *TerraSAR-X Science Team Meeting*. DLR – Oberpfaffenhofen, 25-26 November 2008.

14. Ugsan, D. M., Honda, K. & Saito, G. (2001). Assessment of small passive corner reflectors for geometric correction of radarsat fine mode SAR data. *22nd Asian Conference on Remote sensing*. Singapore, 5-9 November 2001.

15. Kampes, B. M., Hanssen, R. F. & Perski, Z. (2003). Radar Interferometry with public domain tools. In Proc. *Third International Workshop on ERS SAR Interferometry, 'FRINGE03'*. Frascati, Italy, 1-5 Dec. 2003.